Selective Catalytic Hydrogenation of Fatty Acids with Cobalt-halloysite Nanocomposites for Waste Valorization

Alejandro Serrano-Maldonado, Azzedine Bendounan, Mathieu G Silly, Daniel Pla, Montserrat Gómez

ACS Appl. Nano Mater. **2023**, DOI 10.1021/acsanm.3c01361
https://doi.org/10.1021/acsanm.3c01361

Selective Catalytic Hydrogenation of Fatty Acids with Cobalt-halloysite Nanocomposites for Waste Valorization.

Alejandro Serrano-Maldonado,[†] Azzedine Bendounan,[‡] Mathieu G. Silly,[‡] Daniel Pla,[,†] and Montserrat Gómez[*,†].*

[†] Laboratoire Hétérochimie Fondamentale et Appliquée, UMR CNRS 5069, Université Toulouse 3 – Paul Sabatier, 118 route de Narbonne, 31062 Toulouse Cedex 9 (France).

[‡] Synchrotron SOLEIL, L'Orme des Merisiers, 91190 Saint-Aubin (France).

ABSTRACT: Environmentally friendly catalytic composites based on cobalt and a natural clay as catalytically active phase and support respectively, are herein reported for the valorization of fatty acids and esters, in particular for wastes coming from agri-food industry, by selective hydrogenation processes. The as-prepared innovative materials are constituted of zero-valent cobalt nanoparticles immobilized on both pristine halloysite and an ammonium-functionalized clay, with the former support exhibiting better particle distribution on the support as only Co agglomerates could be obtained for ammonium-functionalized halloysite. Under optimized conditions (5 mol% Co, 120 °C, 40 bar), high conversions and remarkable chemoselectivity were observed, leading to the exclusive formation of saturated fatty acids or esters, as well as the formation of tristearin used as a food additive.

KEYWORDS: cobalt nanoparticles, halloysite, catalytic hydrogenation, fatty acid derivatives, waste valorization.

INTRODUCTION

Among the common saturated fatty acids, stearic and palmitic acids are widely present in our daily lives, finding applications in a large variety of products such as emulsifiers, lubricants, surfactants (detergents, soaps, softeners), cosmetics (lotions, creams), candles, and plastics. More specifically, the intake of stearic acid as food supplement has shown to reduce the risk of cardiovascular diseases by lowering both low- and high-density lipoprotein cholesterol concentrations in the blood.[1]

The catalytic hydrogenation of unsaturated fatty acids (mono or poly-unsaturated) is a significant industrial transformation, especially for the production of margarine.[2] As known, most of the hydrogenations applied at industrial scale involve noble metals (such as Pd or Pt) or more abundant Ni-based catalysts (Raney-Ni, Ni-Kieselguhr…), despite the hazards associated to nickel handling.[3, 4] Thus, cobalt-based catalysts could represent an appropriate alternative thanks to their relative low toxicity profiles compared to nickel,[5-7] provided that selective catalytic systems towards C=C hydrogenation can be achieved. Nevertheless, the highest is the content of Co(II), the highest is the selectivity towards hydrodeoxygenation processes as seen for the efficiency of supported cobalt oxide catalysts in the hydrodeoxygenation of fatty acid or esters,[8, 9] albeit under relative high temperature (up to 350 °C) and high pressure (up to 40 bar).[10] Given our interest in the selective hydrogenation of fatty acids for waste valorization purposes, we envisaged the preparation of well-defined zero-valent cobalt nanoparticles immobilized on halloysite to straightforwardly produce saturated fatty acids or esters by C=C bond hydrogenation from fatty wastes. Beller's group reported in 2018 a Co-based heterogeneous catalyst using chitosan as

support, efficiently applied in the hydrogenation of terminal and internal alkenes with high tolerance for different functional groups, including oleic acid.[11] From an industrial point of view, the catalyst robustness and recyclability are crucial aspects to implement innovative catalytic systems at industrial scale. In the literature, few recyclable Co-based catalysts are reported, requiring reactivation treatments given the prone oxidation of Co(0) under ambient conditions.[12]

The design of cobalt nanocatalysts featuring high surface area, low-coordinated metal sites with enhanced reactivity,[13] and metal-support interfaces encompassing key synergistic effects for heterogeneized systems,[14-17] represents an innovative strategy towards catalyst enhancement that has been widely successful for Pd- and Pt-catalyzed hydrogenation systems immobilized both in liquid phase (glycerol[18] and polyols,[19] ionic liquids,[20] deep eutectic solvents[21]…) and solid supports (zeolites,[22, 23] hydrochars,[24] ionic polymers[25] and membranes[26, 27]) thanks to kinetic stabilization of small particles at the nanometric scale, thus preventing deleterious catalyst agglomeration pathways.

In the present work, the immobilization of small cobalt nanoparticles (CoNPs) on halloysite-based supports, both pristine and functionalized halloysite, was successfully attained. These composite materials were efficiently applied in the hydrogenation of mono and poly-unsaturated fatty acids and fatty esters, as well as the hydrogenation of unsaturated C_{18}-rich fatty wastes from duck industry and triolein, leading to tristearin in particular used as a safe food additive.[28] To override deleterious Co(0) oxidation processes which can alter catalyst selectivity (hydrogenation *vs* hydrodeoxygenation), it was possible to take advantage of the magnetic properties of the as-prepared cobalt materials to ease their manipulation and recovery under inert conditions using an external magnet.[29]

EXPERIMENTAL SECTION

The general information is given in the Supporting Information.

Synthesis of quinidine-stabilized cobalt nanoparticles supported on halloysite by decomposition with hydrogen (CoA). A Fisher-Porter bottle was charged with dicobalt octacarbonyl (≥90%) (161.1 mg, 0.42 mmol, 0.85 mmol of Co), quinidine (275.1 mg, 0.85 mmol), halloysite (1000 mg) and sealed with a septum inside the glovebox. The Fisher-Porter bottle was then removed from the glovebox and sealed with its head under argon flow. Degassed EtOH (32 mL) were transferred under Ar with a cannula to the Fisher-Porter bottle to suspend the solids. The system was then pressurized with H_2 (3 bar) at room temperature and then heated at 100 °C (in an oil bath) for 18 h under magnetic stirring. Then, the Fisher-Porter bottle was cooled down to room temperature and depressurized under Ar. A blue greyish dispersion was obtained, which was transferred to a centrifuge tube via cannulation under Ar. Centrifugation was carried out at 3500 rpm for 10 min. After the removal of the supernatant, the solid was redispersed in degassed EtOH (20 mL) and the centrifugation process was repeated for two more times. The obtained gray powder was dried under vacuum overnight and stored in the glovebox prior to use. ICP-AES (Co): 5.6% wt.

Synthesis in polyethyleneglycol dimethylether of cobalt nanoparticles supported on halloysite by decomposition with hydrogen (CoB). A Fisher-Porter bottle was charged with dicobalt octacarbonyl (≥90%) (161.1 mg, 0.42 mmol, 0.85 mmol of Co), halloysite (1000 mg) and sealed with a septum inside the glovebox. The Fisher-Porter bottle was then removed from the glovebox and sealed with its head under Ar. Degassed polyethyleneglycol dimethylether ($MW_{average}$ 240 g/mol, 30 mL) was cannulated under Ar to the Fisher-Porter bottle in order to both solubilize the cobalt precursor and suspend the solids under stirring. The system was then

pressurized with H_2 (3 bar) at room temperature and heated at 120 °C (in a silicon oil bath) for 18 h under magnetic stirring. Then, the Fisher-Porter bottle was cooled down to room temperature and depressurized under Ar. A blue greyish dispersion was obtained, which was transferred to a centrifuge tube *via* cannulation under Ar. Centrifugation was carried out at 3500 rpm for 10 min. After the removal of the supernatant, the solid was redispersed in degassed EtOH (20 mL) and the centrifugation process was repeated for two more times. The obtained gray powder was dried under vacuum overnight and stored in the glovebox prior to use. ICP-AES (Co): 4.3% wt.

Synthesis of cobalt nanoparticles supported on halloysite by reduction with $NaBH_4$ (CoC). A round bottom flask was charged with cobalt acetate (150.5 mg, 0.85 mmol), halloysite (1000 mg), EtOH (30 mL) and stirred at room temperature for 3 h. Then, the solvent was removed under reduced pressure using a rotary evaporator to obtain the cobalt precursor impregnated on halloysite. A solution of $NaBH_4$ (321.5 mg, 8.5 mmol, 10 equiv. to Co) in EtOH (25 mL) was then added dropwise to a dispersion of cobalt-impregnated halloysite in EtOH (10 mL) under constant stirring at room temperature. Upon addition completion, the reaction was stirred at room temperature for 3 h to give a black suspension. The solution was transferred to a centrifuge tube and centrifugation was carried out at 3500 rpm for 10 min. After the removal of the supernatant, the solid was redispersed in EtOH (20 mL) and the centrifugation process was repeated for two times more to remove the excess of $NaBH_4$. The preformed CoNPs on halloysite obtained as gray solid were dried at 80 °C overnight. Subsequently, the preformed CoNPs were transferred to a Fisher-Porter bottle and the system was purged with Ar prior to the cannulation under Ar of degassed EtOH (30 mL) to suspend the solids. The system was then pressurized with H_2 (3 bar) at room temperature and heated at 100 °C (in an oil bath) for 18 h under magnetic stirring. Then, the Fisher-Porter bottle was cooled down to room temperature and depressurized under Ar. A gray

dispersion was obtained, which was transferred to a centrifuge tube *via* cannulation under Ar. Centrifugation was carried out at 3500 rpm for 10 min. After the removal of the supernatant, the obtained gray solid was dried overnight under vacuum and stored in the glovebox prior to use. ICP-AES (Co): 4.61% wt; ICP-AES (B): 0.07% wt.* (depreciable amount); ICP-AES (Na): 0.57% wt.

Synthesis of cobalt nanoparticles supported on halloysite functionalized with *N*,*N*,*N*-triethylpropan-1-aminium iodide (CoD). A Fisher-Porter bottle was charged with dicobalt octacarbonyl (≥90%) (161.1 mg, 0.42 mmol, 0.85 mmol of Co), *N,N,N*-triethylpropan-1-aminium iodide functionalized halloysite (**HAL-Et$_3$I**) (1000 mg) and sealed with a septum inside the glovebox. The Fisher-Porter bottle was then removed from the glovebox and sealed with its head under Ar. Degassed EtOH (32 mL) was cannulated under Ar to the Fisher-Porter bottle to suspend the solids. The system was then pressurized under H_2 (3 bar) at room temperature and heated at 100 °C (in an oil bath) for 18 h under magnetic stirring. Then, the Fisher-Porter bottle was cooled down to room temperature and depressurized under Ar. A blue greyish dispersion was obtained, which was transferred to a centrifuge tube *via* cannulation under Ar. Centrifugation was carried out at 3500 rpm for 10 min. After the removal of the supernatant, the solid was redispersed in degassed EtOH (20 mL) and the centrifugation process was repeated for two more times. The obtained gray powder was dried under vacuum overnight and stored in the glovebox prior to use. ICP-AES (Co): 5.3% wt.

General procedure for catalytic hydrogenation. A 4 mL vial was charged with halloysite-supported Co catalyst (**CoA**, **CoB**, **CoC** or **CoD**, amount as specified in each run), the fatty acid or fatty ester starting material (1 mmol) and a stirring bar under Ar inside a glovebox. The vial was closed with a septum prior to be taken out of the glovebox and placed inside a 50 mL autoclave

(TOP Industrie S.A.S.). Then the septum of the vial was removed and the autoclave was immediately purged with Ar at room temperature prior to being charged with H_2 (specified pressure in each run). The autoclave then was placed in a pre-heated aluminum block at 80 °C on a heating plate equipped with a magnetic stirrer. The reaction mixture was then heated at the selected temperature for the specified reaction time in each run. The aluminum block was then removed, the autoclave was allowed to cool down to room temperature and the remaining hydrogen pressure was carefully released. Taking advantage of the magnetic behavior of catalyst, the reaction crudes were extracted with ethyl acetate (3 x 5 mL) using an external magnet to easily separate the catalyst from the supernatant. After solvent removal under reduced pressure, 1,4-dimethoxybenzene (1 equiv.) was added as internal standard (1 equiv.), and ^{1}H NMR in $CDCl_3$ was performed for determination of reaction conversion and selectivity. Moreover, GC FID analysis of reaction crudes was directly performed for fatty ester substrates. Indirect GC FID analysis of reactions using fatty acid substrates, was performed after methanol esterification under acidic conditions as reported in the literature [30]. In both cases, reaction selectivity towards alkyl stearate were estimated via integration of peak areas corresponding to the alkyl stearate derivative versus other unsaturated esters.

Catalyst recycling procedure. Following the general procedure for catalytic reactions using catalyst **CoC** (63.9 mg, 5 mol%) and methyl oleate (296.5 mg), 80 °C and 4 h reaction times were chosen for each reaction run. A mixture heptane/ethyl acetate (5:1, 5 mL × 3) was used for reaction crude extraction after each run and the recovered catalyst was dried under vacuum and kept under Ar before each consecutive run. The loading of fresh methyl oleate substrate (296.5 mg) was done under ambient conditions. ICP-AES analysis of all organic fractions was carried-out.

RESULTS AND DISCUSSION

Synthesis and characterization of catalytic materials. With the aim of efficiently immobilizing cobalt nanoparticles (CoNPs) on halloysite-based supports, different materials were prepared using both unfunctionalized and ammonium-functionalized halloysite; the latter was prepared following our previous reported methodology (Figure 1).[31]

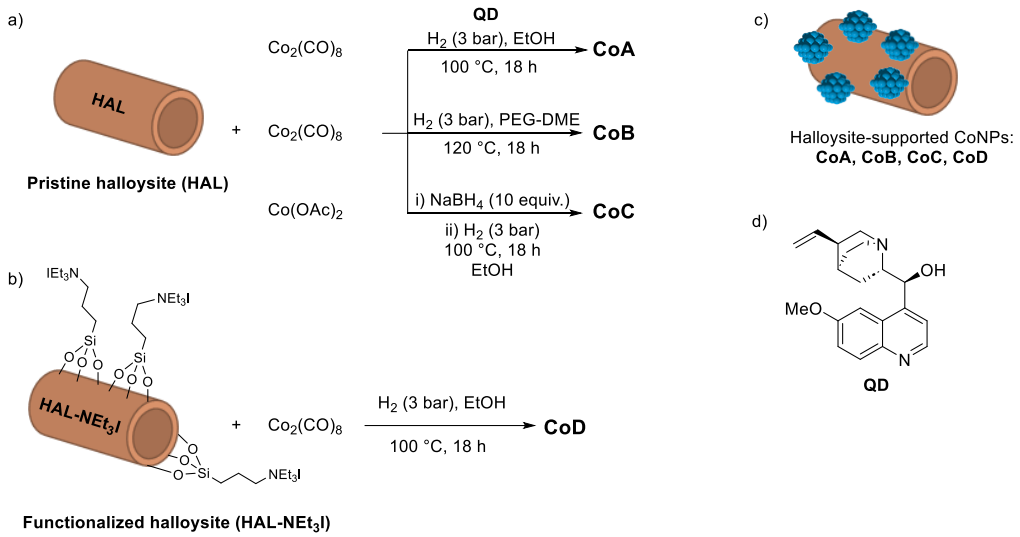

Figure 1. a) Synthesis of Co-based nanocomposites supported on pristine halloysite (**CoA**, **CoB**, **CoC**); b) synthesis of Co-based nanocomposites supported on a tetraalkylammonium functionalized halloysite (**CoD**); c) schematic representation of CoNPs immobilized on halloysite-based supports; d) chemical structure of quinidine.

Using the pristine clay, three approaches were envisaged taking into account the influence of the metal precursor [$Co_2(CO)_8$, $Co(OAc)_2$], and the nature of both the stabilizing agent [quinidine, polyethyleneglycol dimethylether (PEG-DME)] and the reducing agent (H_2, $NaBH_4$). In order to study the influence of the two stabilizers in the synthesis of **CoC** and thus to compare the catalytic behavior with **CoA** and **CoB** (see below Co-catalyzed hydrogenation discussion), we added QD and PEG-DME in two independent controls using $Co(OAc)_2$ as metallic precursor. Unfortunately,

the materials obtained in both cases were not well-defined. Whereas the corresponding metal nanoparticles were not adsorbed on the support, leading to two immiscible solid phases using quinidine; the use of PEG-DME instead of ethanol was not possible due to the lack of solubility of $Co(OAc)_2$ in this medium.

As observed by TEM analyses, the presence of quinidine led to small nanoparticles uniformly distributed on the halloysite (3.2 ± 0.9 nm; dispersion of 23%, see Supporting Information for the dispersion determination) (**CoA**, Figure 2a), in agreement with our previous contributions involving metal nanoparticles.[31-33] However, in the presence of PEG-DME, non-uniformly distributed nanoparticles on the support were obtained (**CoB**) with sizes ranging between 13-30 nm, evidencing that PEG-DME (average MW 240 g/mol) was not a suitable stabilizer (Figure 2b). Furthermore, it is worth to mention that molecular hydrogen was not able to reduce $Co(OAc)_2$ precursor. Thus, we used sodium tetrahydroborate as reducing agent, followed by hydrogen treatment; this strategy led to homogenously distributed CoNPs on halloysite (**CoC**, Figure 2c), attaining small sizes with a narrow distribution (2.9 ± 0.4 nm; dispersion of 25%, see Supporting Information for the dispersion determination). Besides, the alternative strategy using the tetraalkylammonium-functionalized halloysite aiming at a plausible electrostatic stabilization of CoNPs by the ammonium moieties was discarded as only cobalt agglomerates were obtained for **CoD** (Figure 2d).

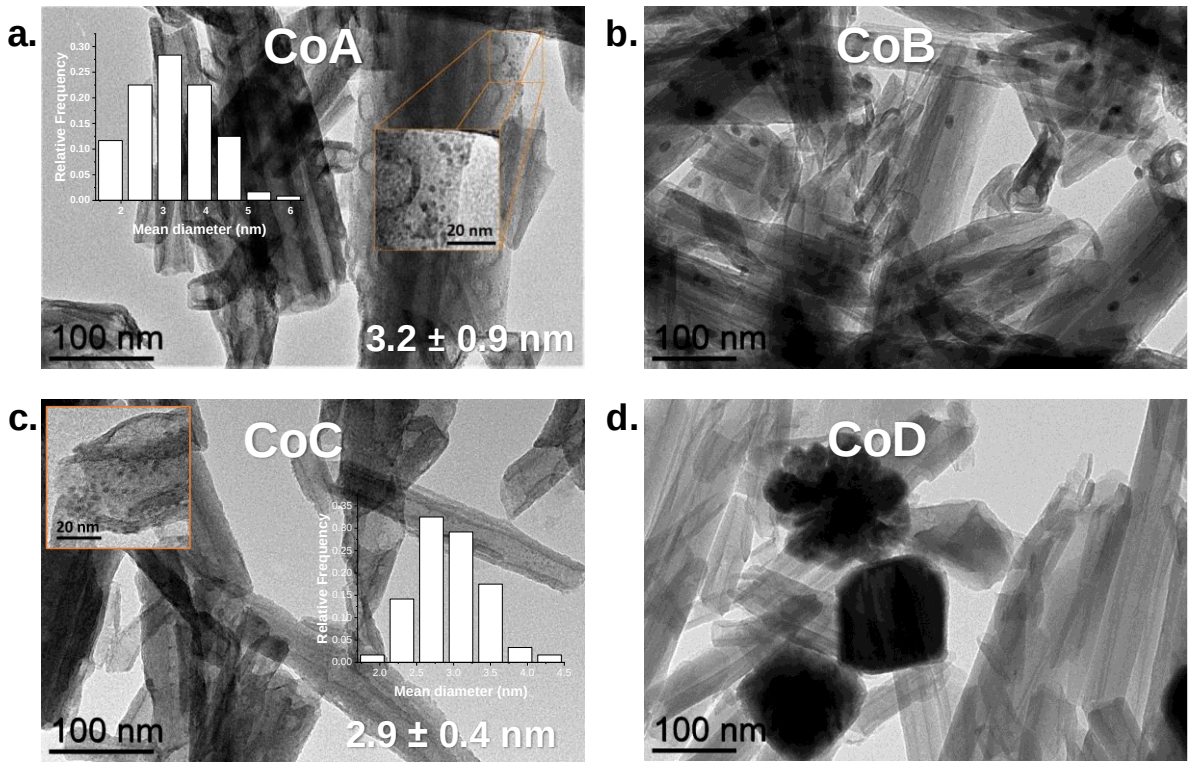

Figure 2. TEM micrographs of halloysite-supported cobalt catalytic materials of: (a) **CoA** with magnification and particle size distribution (3.2 ± 0.9 nm for 120 nanoparticles); (b) **CoB** (particle sizes between 13-30 nm); (c) **CoC** with magnification and particle size distribution (2.9 ± 0.4 nm for 120 nanoparticles); (d) **CoD** (only agglomerates observed) (see Figures S1-S4 in the Supporting Information for more TEM micrographs of each material).

ICP-AES analyses of the as-prepared materials corroborated the efficient deposition of Co over the halloysites (see Table S1 in the Supporting Information): 5.6 wt% for **CoA**, 4.3 wt% for **CoB**, 4.6 wt% for **CoC,** and 5.3 wt% for **CoD** (expected data: 5 wt%). In addition, for **CoC**, no boron was detected by ICP-AES, but a small amount of sodium remained (0.6 wt%). Elemental analyses of **CoA** and **CoD** evidenced the presence of quinidine and ammonium groups respectively (N content: 0.30 wt% for **CoA** and 0.31 wt% for **CoD**; N content of support **HAL-NEt$_3$I**: 0.34 wt%) (see Table S1 in the Supporting Information). Powder X-ray diffraction analyses of **CoA-CoC**

only showed the corresponding peaks of halloysite, probably due to the small amount of cobalt together with potential peak broadening effects due to the small size of CoNPs, in particular for **CoA** and **CoC** (see Figure S5 in the Supporting Information). No further characterization of **CoD** was carried out due to the lack of stabilization of ammonium groups.

With the aim of evidencing the functional groups present on the as-prepared Co-based materials coming from stabilizers, FTIR analyses were carried out (Figures S6-S10). For **CoA**, absorption bands corresponding to C–H stretching (ca. 3000-2840 cm^{-1}) were clearly identified together with bands in the region ca. 1630-1450 cm^{-1}, corroborating the presence of quinidine (see Figure S6 in the Supporting Information). For **CoB**, absorption bands corresponding to C–H stretching (ca. 3000-2840 cm^{-1}) and C–O stretching (1100 cm^{-1}) were observed (see Figure S7 in the Supporting Information), indicating that PEG-DME was still present in the material despite the several ethanol washes carried out. For **CoC**, absorption bands in the region of 1650 and 1450 cm^{-1} were observed, indicating the presence of coordinated acetate groups; their presence can be responsible of the stabilization of nanoparticles by an electrostatic effect during synthesis (see Figures S8-S9 in the Supporting Information).[34, 35] It is important to highlight that after the first step of the **CoC** synthesis (*i.e.* prior treatment with H_2; Figure 1), a mixture of acetates species (coordinated and ionic) are present in the material, but not after the second step (*i.e.* after treatment with H_2; Figure 1). FTIR spectra of both **CoD** and the functionalized support **HAL-NEt$_3$I** exhibited the same absorption bands, indicating that the functionalization remains after immobilization of cobalt (see Figure S10 in the Supporting Information).

For those materials exhibiting the presence of nanoparticles, *i.e.* **CoA**, **CoB** and **CoC**, specific surface areas of **CoA**, **CoB** and **CoC** were determined (51.6, 19.0 and 50.3 m^2g^{-1}, respectively). Furthermore, magnetic measurements of **CoA**, **CoB** and **CoC** at 2 K were carried out (see Figure

S11 in the Supporting Information). **CoA** and **CoB** exhibited hysteresis with coercive fields of 445 and 469 Oe, and saturation magnetization (M_s) of 102.2 and 66.8 emu/g respectively, showing a weak ferromagnetic behavior (see Figure S11a and S11b in the Supporting Information). The values of M_s were lower than that reported for bulk Co-*hcp* (162 emu/g),[36] probably due to either the capping effect triggered by stabilizers over the surface of cobalt nanoparticles due to surface spin capping effects[37, 38] or the presence of cobalt oxides for **CoA** and **CoB**.[39-42] Moreover, **CoC** exhibited higher coercive field (1235 Oe) and higher saturation magnetization (248 emu/g) than **CoA** and **CoB** (see Figure S11c in the Supporting Information), evidencing a less saturated surface (absence of stabilizers in agreement with the behavior reported for cobalt clusters and nanoparticles).[37, 43]

The X-ray Absorption Spectroscopy (XAS) analyses of **CoA** and **CoB** confirmed the presence of cobalt oxidized phases, mainly Co(II) attributed to CoO (Figure 3a). The absorption spectra of **CoA** and **CoB** are comparable to the reported for CoO nanocrystals.[44] In contrast, **CoC** was mostly constituted of Co(0) (Figure 3b).

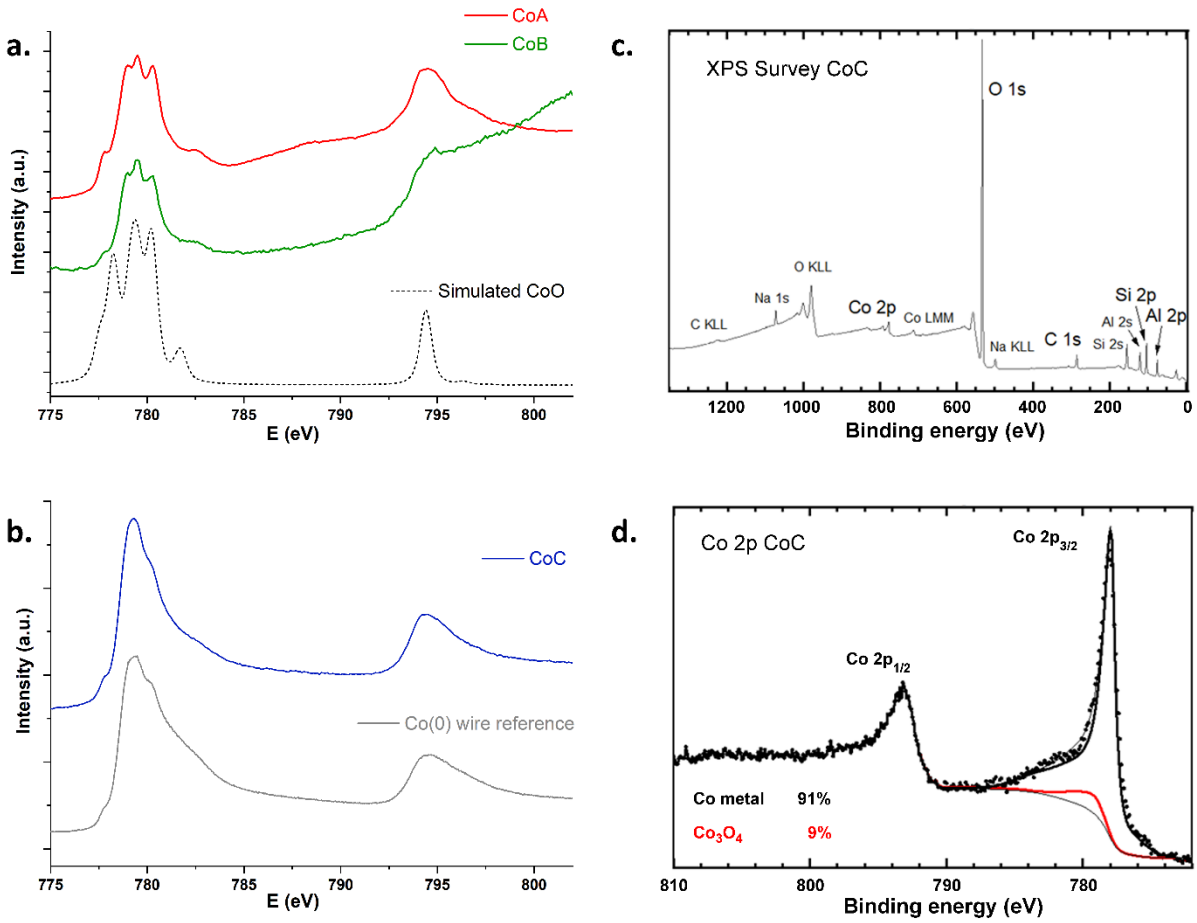

Figure 3. Cobalt $L_{2,3}$ XAS spectra: (a) **CoA** (red), **CoB** (green) and an atomic multiplet simulation of CoO (black dotted line); (b) **CoC** (blue) and Co(0) reference (grey). XPS analysis of **CoC**: (c) XPS survey spectrum. (d) High-resolution spectrum at the binding region of Co 2p; black and red continuous traces correspond to Co(0) and Co_3O_4 envelopes used to fit the experimental data (dotted line); the fit was carried out on the Co $2p_{3/2}$ binding energy.

Considering the catalytic performance of **CoC** (see below, section 3.2), further characterization of this material was performed. X-ray photoelectron spectroscopy (XPS) analysis was carried out to determine the elements present at the surface of the catalytic material as well as the oxidation state of cobalt species immobilized on halloysite (Figures 3c and 3d). The XPS survey spectrum showed the presence of Al, O, and Si from the halloysite support and also the presence of Na

coming from the first step of its synthesis, along with Co; no boron was detected. The analysis at the binding energy corresponding to Co 2p region evidenced that nanoparticles are mainly constituted of Co(0) (91%) with only 9% of the mixed oxide Co_3O_4 [constituted of Co(II) and Co(III)] (see Figure S12 and Table S2 in the Supporting Information for more information about the quantification procedure).

Fast Fourier Transform (FFT) treatment on a HRTEM image corresponding to a nanoparticle evidenced the presence of Co(0) with a *hcp* crystal structure [(4,1,1), (1,1,4) and (0,0,4] crystallographic planes] (see Figure 4 and Figure S13 in the Supporting Information for a complete list of measured crystallographic planes). Additionally, the EDX (Energy Dispersive X-ray spectroscopy) mapping showed the uniformly distribution of cobalt over the halloysite surface (see Figure S14 in the Supporting Information).

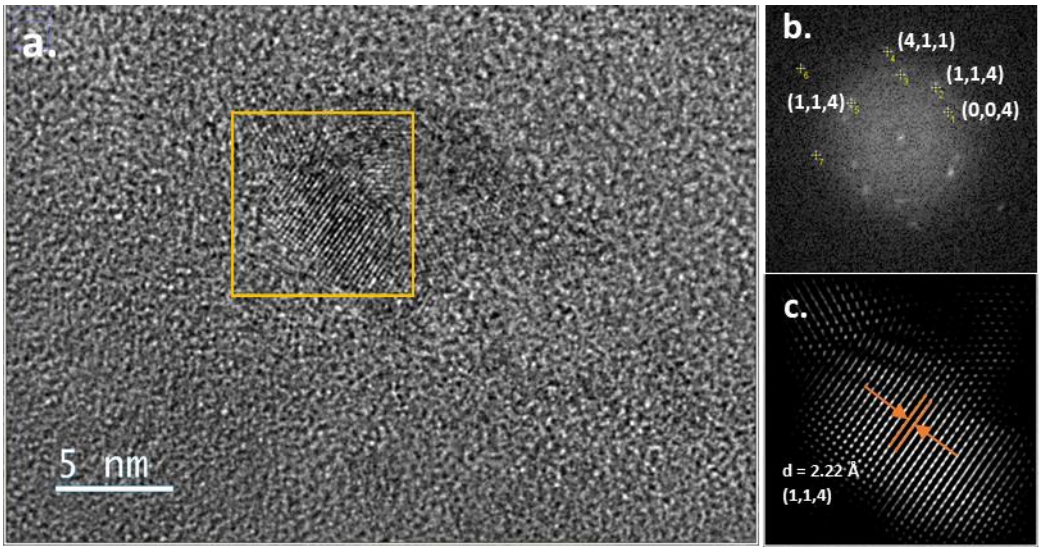

Figure 4. (a) HRTEM image of **CoC** (framed area corresponding to FFT analysis); (b) FFT showing crystallographic planes of Co(0) hcp structure; (c) inversed FFT of (b) evidencing in particular the crystallographic plane (1,1,4).

Co-catalyzed hydrogenation processes. The as-prepared catalytic materials were applied in the benchmark hydrogenation of oleic acid (**1**) to give stearic acid (**2**), in order to compare their relative catalytic behavior (Table 1). Under neat conditions, working at 250 °C and 40 bar H_2 pressure, **CoD** was the less active catalyst (entries 4 vs 1-3, Table 1), as expected for the presence of large Co agglomerates in the catalytic material. At 180 °C, the activity of **CoA** dropped to 42% conversion (entry 5, Table 1), in contrast to **CoB** and **CoC** which maintained a high activity (more than 88%, entries 6-7, Table 1). From this trend, it seems that quinidine acting as stabilizer of the CoNPs in the **CoA** catalytic material hampers the hydrogenation of oleic acid, probably due to a stronger interaction with the metal surface than the fatty acid. At lower temperature, the most active catalytic system was **CoC**, giving more than 90% conversion at 120 °C and even 62% at 100 °C (entries 9 and 11, Table 1); however, **CoB** exhibited a lower activity below 180 °C (entries 8 and 10, Table 1). From this comparative study, the catalytic material **CoC**, prepared from $Co(OAc)_2$ as precursor in the absence of stabilizing agent other than the unfunctionalized halloysite, led to the better catalytic activity and selectivity (in all the cases, only stearic acid is formed); after 6 h of reaction, the conversion was still relatively high (>60%, entry 12, Table 1). The addition of quinidine or PEG-DME to **CoC** (stabilizers used in the synthesis of **CoA** and **CoB**, respectively) deactivated the catalytic system (see Scheme S1 in the Supporting Information).

Working at lower pressure (20 bar), the activity dropped from 91% conversion to 39% (entry 9 vs 13, Table 1). A decrease in cobalt loading (2.5 mol%) also triggered an activity loss (entry 9 vs 14, Table 1). No significant adsorption of fatty acids or fatty esters was observed by infrared spectroscopy (see Figure S15 in the Supporting Information), recovering quantitatively the organic compounds, in contrast to the composite material halloysite/stearic acid described in the literature.[45]

Moreover, we desired to elucidate the impact of the hydrogenation treatment during the synthesis of **CoC** (Figure 1). For this purpose, the material coming from the first-step (*i.e.* the material obtained after reduction of $Co(OAc)_2$ with $NaBH_4$) was evaluated in the hydrogenation of oleic acid. After reaction, the substrate was quantitatively recovered, proving the importance of the activation step (*i.e.* H_2 treatment, which corresponds to the second step of the preparation of **CoC**) to generate the catalytically active species (see Figure S16 in the Supporting Information).

Table 1. Co-catalyzed hydrogenation of oleic acid using **CoA**, **CoB**, **CoC** and **CoD**.[a]

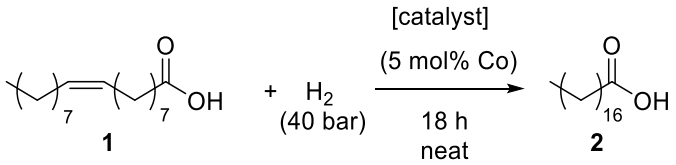

Entry	Catalyst	T (°C)	Conv. (%)[b]
1	**CoA**	250	95
2	**CoB**	250	96
3	**CoC**	250	>99
4	**CoD**	250	18
5	**CoA**	180	42
6	**CoB**	180	88
7	**CoC**	180	>99
8	**CoB**	120	52
9	**CoC**	120	91
10	**CoB**	100	18
11	**CoC**	100	62
12[c]	**CoC**	120	63
13[d]	**CoC**	120	39
14[e]	**CoC**	120	57

[a] Reaction conditions: 1 mmol of oleic acid (**1**), 0.05 mmol of total Co (determined by ICP-AES). [b] Determined by ^{1}H NMR using 1,4-dimethoxybenzene as internal standard. Only stearic acid was observed. [c] 6 h of reaction. [d] 20 bar H_2 pressure. [e] 2.5 mol% cobalt.

The high content of cobalt oxidized phases, mainly CoO, for **CoA** and **CoB** (as evidenced by XAS), in contrast to **CoC** that contains more than 90% of Co(0) as determined by XPS quantification,[44] resulted in differential catalyst behaviors. Notably, both **CoA** and **CoB** were more active at high temperature (250 °C) than at relative low temperatures [<180 °C for **CoA** (entry 5 *vs* 1, Table 1); <120 °C for **CoB** (entry 8 *vs* 2, Table 1)], probably due to the reduction of cobalt species at relative high temperatures; **CoC** preserved its activity even at 100 °C (entry 11, Table 1). This structural feature corroborates that Co(0) species are responsible of the C=C bond hydrogenation.

Thus, we can conclude that both Co(0) oxidation state (**CoA** and **CoB** are less active than **CoC**) and relatively small nanoparticle sizes (**CoB** is less active than **CoC**) of the as-prepared composite materials are crucial aspects to induce catalytic reactivity in the hydrogenation of fatty acids. Furthermore, **CoC** exhibits higher reactivity than other related first-row metal catalysts, and comparable catalytic behavior regarding NiNPs immobilized on halloysite previously reported by our team (see Table S3 in the Supporting Information).

Under the optimized conditions (**CoC**, 5 mol% Co, 120 °C, 40 bar H_2), other C_{18} unsaturated fatty acids were hydrogenated (**3-5**, Table 2). Elaidic acid (**3**), the (*E*)-isomer of oleic acid, could be hydrogenated giving 87% of stearic acid (entry 1, Table 2). Linoleic and linolenic acids containing two and three C=C bonds respectively, were also efficiently reduced, yielding more than 88% of stearic acid together with low amounts of unsaturated acids (2-5%; entries 3-4, Table 2).

Table 2. CoC-catalyzed hydrogenation of C_{18} unsaturated fatty acids.[a]

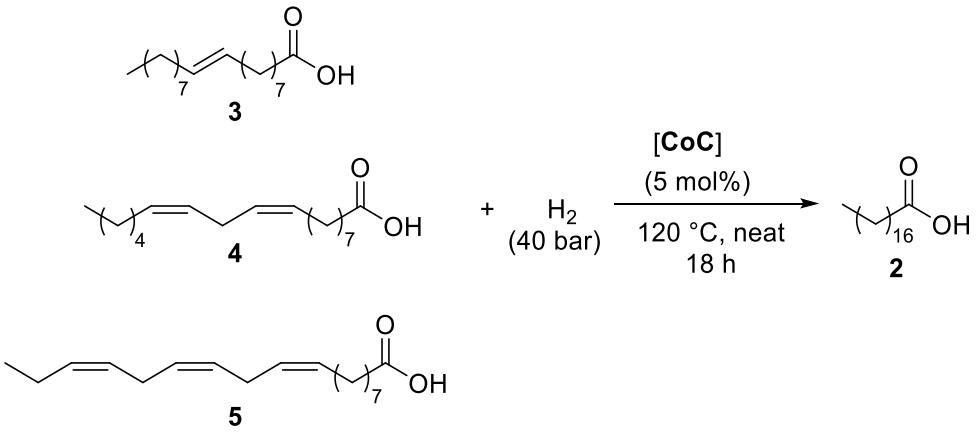

Entry	Substrate	Conv. (%)[b]
1	**3**	87
2[c]	**3**	35
3	**4**	95(93)[d]
4	**5**	93(88)[d]

[a] Reaction conditions: 1 mmol of substrate, 0.05 mmol of total Co (determined by ICP), neat. [b] Conversion determined by ^{1}H NMR using 1,4-dimethoxybenene as internal standard. [c] After 6 h reaction. [d] In brackets, stearic acid (%) determined by GC-FID after esterification of fatty acids with methanol (methyl esters).

For oleic acid and elaidic acid, we were interested in evidencing the plausible *E/Z* isomerization under hydrogenation conditions.[46, 47] At relative short reaction times (6 h), *E/Z* isomerization was observed by ^{13}C NMR (298 K) for both fatty acids (see Figure S17 in the Supporting Information). This behavior points to a more favored C=C bond adsorption than C=O bond adsorption in agreement with the absence of C=O reduced compounds, as previously observed for Co-based heterogeneous catalysts applied to the isomerization of methyl *cis*-9-octadecenoate.[48]

With the aim of eluding the plausible corrosive effects using fatty carboxylic acids as substrates, we studied the efficiency of **CoC** in the hydrogenation of methyl fatty esters (**6**, **7**) (Table 3). As expected,[49] the C=C bond hydrogenation of methyl oleate was favored compared to oleic acid

(Table 1), obtaining quantitative conversions at relative low temperature (entries 1-2, Table 3). Decreasing the cobalt loading, the activity dramatically decreased (only 17% conversion; entry 3, Table 3). At 80 °C and short reaction times, the activity kept high (entries 4-6, Table 3). Methyl linoleate was also hydrogenated, but 120 °C was required to fully hydrogenated the two C=C bonds of the substrate (entry 8, Table 3); at 80 °C, a high amount of unsaturated products was obtained (entry 7, Table 3).

Table 3. CoC-catalyzed hydrogenation of methyl fatty esters.[a]

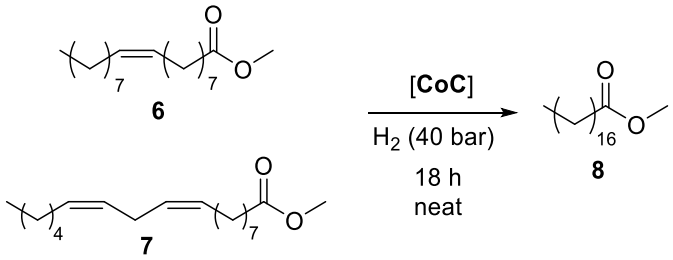

Entry	Substrate	Co loading (mol%)	Time (h)	T (° C)	Conv. (%)[b]
1	**6**	5	18	120	>99[c]
2	**6**	5	18	80	>99[c]
3	**6**	1	18	80	17[c]
4	**6**	5	6	80	99[c]
5	**6**	5	4	80	88[c]
6	**6**	5	3	80	50[c]
7	**7**	5	18	80	62(11)[d,e]
8	**7**	5	4	120	>99(99)[d]

[a] Reaction conditions: 1 mmol of substrate, 0.05 mmol of total Co (determined by ICP), neat. [b] Determined by ^{1}H NMR using 1,4-dimethoxybenene as internal standard. [c] Only methyl stearate was observed. [d] In brackets, methyl stearate (%) determined by GC-FID. [e] 51 % of unsaturated products.

Taking advantage of the magnetic behavior of **CoC**, we assessed the reusability of the catalyst towards the hydrogenation of methyl oleate with the help of an external magnet to facilitate the workup procedure and minimize catalyst oxidation albeit such manipulations were done in air (see Figure S18 in the Supporting Information). The catalyst was straightforwardly reused up to the third run, maintaining 50% conversion after the fifth run (Figure 5). The cobalt content on the organic products was depreciable (0.01 ppm) after each catalytic run (determined by ICP-AES), discarding the loss of activity due to leaching. TEM analyses after the 7th catalytic run reveals the presence of large cobalt agglomerates together with well-distributed nanoparticles over the halloysite (see Figure S19 in the Supporting Information), probably being the cause of drop in activity. Furthermore, elemental analysis of **CoC** catalyst before and after catalysis revealed 1.5 times higher C content after the first run than the original C content present in the fresh nanomaterial composite after synthesis (1.30% C after the first run vs 0.84% C in the **CoC** fresh catalyst), effect that can also contribute to the deactivation of the catalyst.

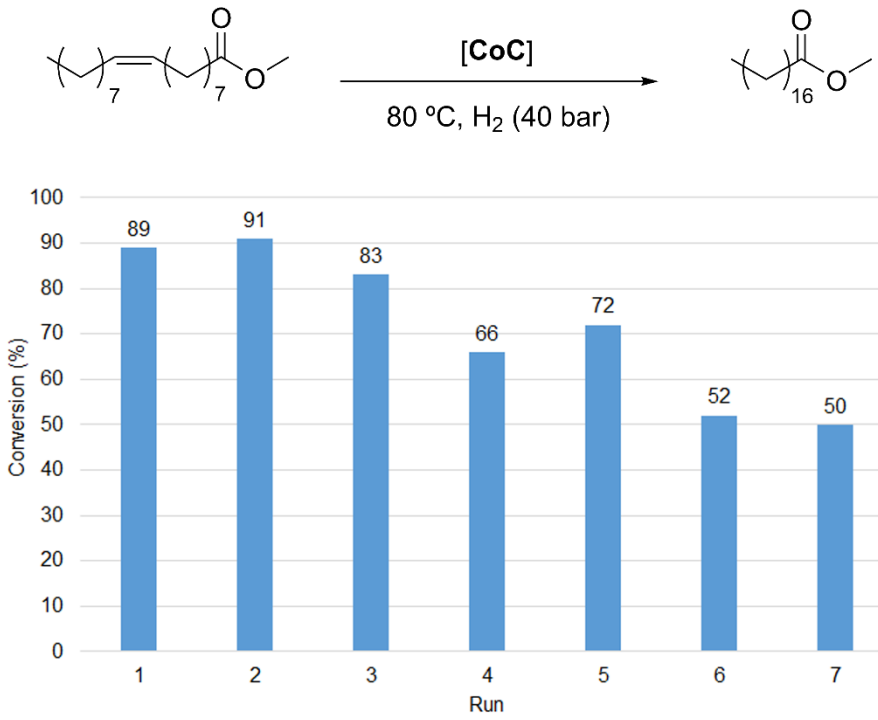

Figure 5. **CoC**-catalyzed hydrogenation of methyl oleate and the corresponding recycling using an external magnet.

From an application viewpoint, we were interested in the **CoC**-catalyzed hydrogenation of triolein (**9**), the triglyceride of oleic acid, because its saturated product, tristearin (**10**), is considered as a safe food additive and is also used as hardening stabilizer in the production of soaps. We succeeded in obtaining tristearin in quantitative yield under neat conditions and smoother conditions than previously reported cobalt nanoparticles immobilized on chitosan (Scheme 1).[11]

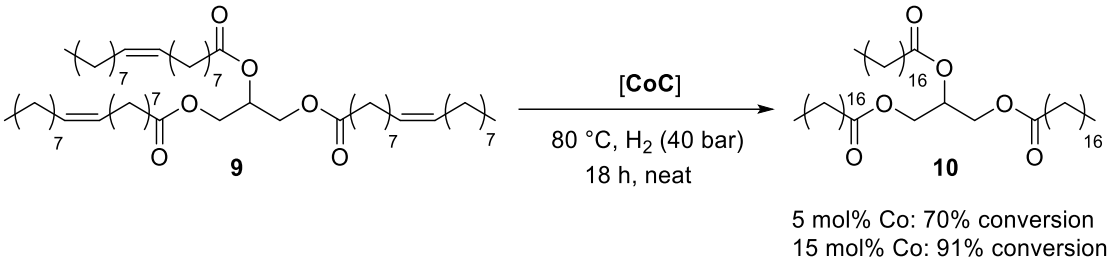

Scheme 1. **CoC**-catalyzed triolein hydrogenation. Reaction conditions: 0.33 mmol of substrate, 0.0165 or 0.05 mmol of total Co (determined by ICP). Conversions determined by ^{1}H NMR using 1,4-dimethoxybenene as internal standard.

Upon completion of the optimization studies and scope starting from pure substrates, we explored the catalytic valorization of mixtures of fatty wastes from agri-food industries, in particular from duck industry (sample supplied by SAPOVAL company), using the best catalyst composite (see Table S4 in the Supporting Information). Thus, **CoC** showed high efficiency in the hydrogenation of duck fatty wastes, mainly constituted of C_{18} unsaturated acids (see Figure S20 in the Supporting Information). At 120 °C for 18 h using 5 mol% cobalt under 40 bar H_2, the hydrogenation of the waste was up to 93%. When this mixture was previously esterified with methanol, the time was clearly reduced (4 h) obtaining a quantitative hydrogenation of the esterified waste, mainly constituted of 32% of methyl palmitate (C_{16}) and 68% of methyl stearate (C_{18}). Moreover, only 0.2 ppm of cobalt was detected by ICP-AES in the hydrogenated products.

CONCLUSIONS

To sum up, original Co/halloysite composites containing cobalt-based nanoparticles were prepared by an organometallic approach, leading to well-defined materials, mainly depending on both the nature of reagents and the support functionalization, which were fully characterized

[(HR)TEM, PXRD, FTIR, XPS, XAS, magnetization, ICP, specific surface area]. Four catalytic materials were prepared, those using unfunctionalized halloysite showed the formation of Co-based nanoparticles of different sizes and distribution on the supports (**CoA**, **CoB**, **CoC**), whereas the one prepared using the ammonium-functionalized clay led mostly to agglomerates (**CoD**). By appropriately adjusting the reaction parameters, we managed to synthesize a material containing small zero-valent CoNPs (*ca*. 3 nm of mean diameter), well-distributed on pristine halloysite and in the absence of any stabilizer other than the support (**CoC**). The oxidation state of the immobilized cobalt nanoparticles on halloysite (determined by XPS and XAS) appeared crucial to understand their catalytic reactivity, being those mainly constituted of Co(II), **CoA** and **CoB**, less efficient that the nanocomposite based on Co(0), **CoC**; this structural feature reveals that Co(0)-based nanoparticles are catalytically active in the hydrogenation of C=C bonds.

CoC was successfully applied in the selective C=C bond reduction of mono- and poly-unsaturated C_{18} fatty acids and esters, including those coming from industrial wastes and finding applications in the synthesis of value added products, such as tristearin.

ASSOCIATED CONTENT

Supporting Information. General experimental section; characterization of catalyst(s) (TEM, ATR, PXRD, FFT with list of measured distances, HAADF-STEM with EDX mapping, XPS of cobalt standards for quantification); ATR of catalyst after reaction(s); ^{13}C NMR spectra of isomerization studies; photograph of magnetic separation of catalyst; TEM of **CoC** after seven reuses; table with elemental analysis and ICP-AES data of catalytic materials; table with XPS quantification data of **CoC**; NMR spectra of fatty waste and reaction products (^{1}H and ^{13}C NMR); and selected examples of monitoring of fatty acid or fatty ester hydrogenation (^{1}H NMR and GC) (PDF).

AUTHOR INFORMATION

Corresponding Authors

Daniel Pla - *Laboratoire Hétérochimie Fondamentale et Appliquée, UMR CNRS 5069, Université Toulouse 3 – Paul Sabatier, 118 route de Narbonne, 31062 Toulouse Cedex 9 (France)*. https://orcid.org/0000-0002-8703-8778. *Email: pla@lhfa.fr

Montserrat Gómez - *Laboratoire Hétérochimie Fondamentale et Appliquée, UMR CNRS 5069, Université Toulouse 3 – Paul Sabatier, 118 route de Narbonne, 31062 Toulouse Cedex 9 (France)*. https://orcid.org/0000-0003-1211-1333. * Email: montserrat.gomez-simon@univ-tlse3.fr

Authors

Alejandro Serrano-Maldonado - *Laboratoire Hétérochimie Fondamentale et Appliquée, UMR CNRS 5069, Université Toulouse 3 – Paul Sabatier, 118 route de Narbonne, 31062 Toulouse Cedex 9 (France)*. https://orcid.org/0000-0003-3076-854X.

Azzedine Bendounan - *Synchrotron SOLEIL, L'Orme des Merisiers, 91190 Saint-Aubin (France).* https://orcid.org/0000-0001-7557-4322

Mathieu G. Silly - *Synchrotron SOLEIL, L'Orme des Merisiers, 91190 Saint-Aubin (France).* https://orcid.org/0000-0002-0302-8442.

Notes

The authors declare no competing financial interest.

ACKNOWLEDGMENTS

The Centre National de la Recherche Scientifique (CNRS) and the Université Toulouse 3-Paul Sabatier are gratefully acknowledged for their financial support. Authors thank POCTEFA Interreg program for funding this work (EFA308/19 TRIPyr). We acknowledge SOLEIL for provision of synchrotron radiation facilities at TEMPO beamline, proposal number 20220626. Christian Pradel and Lénaïc Madec are acknowledged for the (HR)TEM and XPS analyses and helpful discussions, respectively. Authors thank Laetitia Cavaillé and Erwan Trotoux from Sapoval for providing industrial fatty waste samples.

REFERENCES

(1) van Rooijen, M. A.; Mensink, R. P. Palmitic Acid Versus Stearic Acid: Effects of Interesterification and Intakes on Cardiometabolic Risk Markers—A Systematic Review. *Nutrients* **2020**, *12*, 615, https://doi.org/10.3390/nu12030615.

(2) List, G. R.; King, J. W. *Hydrogenation of Fats and Oils: Theory and Practice*; AOCS Press, 2015.

(3) Genchi, G.; Carocci, A.; Lauria, G.; Sinicropi, M. S.; Catalano, A. Nickel: Human Health and Environmental Toxicology. *Int. J. Environ. Res. Public Health* **2020**, *17*, 679, https://doi.org/10.3390/ijerph17030679.

(4) Yang, P.; Zhang, L. J.; Wang, X. J.; Wang, Z. L. Exploring the management of industrial hazardous waste based on recent accidents. *J. Loss Prev. Process Ind.* **2020**, *67*, 104224, https://doi.org/10.1016/j.jlp.2020.104224.

(5) Leyssens, L.; Vinck, B.; Van Der Straeten, C.; Wuyts, F.; Maes, L. Cobalt toxicity in humans-A review of the potential sources and systemic health effects. *Toxicology* **2017**, *387*, 43-56, https://doi.org/10.1016/j.tox.2017.05.015.

(6) Unice, K. M.; Monnot, A. D.; Gaffney, S. H.; Tvermoes, B. E.; Thuett, K. A.; Paustenbach, D. J.; Finley, B. L. Inorganic cobalt supplementation: Prediction of cobalt levels in whole blood and urine using a biokinetic model. *Food Chem. Toxicol.* **2012**, *50*, 2456-2461, https://doi.org/10.1016/j.fct.2012.04.009.

(7) Tvermoes, B. E.; Paustenbach, D. J.; Kerger, B. D.; Finley, B. L.; Unice, K. M. Review of cobalt toxicokinetics following oral dosing: Implications for health risk assessments and metal-on-metal hip implant patients. *Crit. Rev. Toxicol.* **2015**, *45*, 367-387, https://doi.org/10.3109/10408444.2014.985818.

(8) Zhou, Y.; Liu, L.; Li, G.; Hu, C. Insights into the Influence of ZrO_2 Crystal Structures on Methyl Laurate Hydrogenation over Co/ZrO_2 Catalysts. *ACS Catal.* **2021**, *11*, 7099-7113, https://doi.org/10.1021/acscatal.1c00632.

(9) Song, S.; Wang, D.; Di, L.; Wang, C.; Dai, W.; Wu, G.; Guan, N.; Li, L. Robust cobalt oxide catalysts for controllable hydrogenation of carboxylic acids to alcohols. *Chin. J. Catal.* **2018**, *39*, 250-257, https://doi.org/10.1016/s1872-2067(17)63003-1.

(10) Zula, M.; Grilc, M.; Likozar, B. Hydrocracking, hydrogenation and hydro-deoxygenation of fatty acids, esters and glycerides: Mechanisms, kinetics and transport phenomena. *Chem. Eng. J.* **2022**, *444*, 136564, https://doi.org/10.1016/j.cej.2022.136564.

(11) Scharnagl, F. K.; Hertrich, M. F.; Ferretti, F.; Kreyenschulte, C.; Lund, H.; Jackstell, R.; Beller, M. Hydrogenation of terminal and internal olefins using a biowaste-derived heterogeneous cobalt catalyst. *Sci. Adv.* **2018**, *4*, eaau1248/1241, https://doi.org/10.1126/sciadv.aau1248.

(12) Audemar, M.; Ciotonea, C.; Vigier, K. D. O.; Royer, S.; Ungureanu, A.; Dragoi, B.; Dumitriu, E.; Jerome, F. Selective Hydrogenation of Furfural to Furfuryl Alcohol in the Presence of a

Recyclable Cobalt/SBA-15 Catalyst. *ChemSusChem* **2015**, *8*, 1885-1891, https://doi.org/10.1002/cssc.201403398.

(13) Iablokov, V.; Beaumont, S. K.; Alayoglu, S.; Pushkarev, V. V.; Specht, C.; Gao, J.; Alivisatos, A. P.; Kruse, N.; Somorjai, G. A. Size-Controlled Model Co Nanoparticle Catalysts for CO_2 Hydrogenation: Synthesis, Characterization, and Catalytic Reactions. *Nano Lett.* **2012**, *12*, 3091-3096, https://doi.org/10.1021/nl300973b.

(14) Zhu, Y.; Ye, Y.; Zhang, S.; Leong, M. E.; Tao, F. Synthesis and catalysis of location-specific cobalt nanoparticles supported by multiwall carbon nanotubes for Fischer-Tropsch synthesis. *Langmuir* **2012**, *28*, 8275 - 8280, https://doi.org/10.1021/la300607k.

(15) Mamontova, E.; Trabbia, C.; Favier, I.; Serrano-Maldonado, A.; Ledeuil, J.-B.; Madec, L.; Gómez, M.; Pla, D. Novel Catalyst Composites of Ni- and Co-Based Nanoparticles Supported on Inorganic Oxides for Fatty Acid Hydrogenations. *Nanomaterials* **2023**, *13*, 1435, https://doi.org/10.3390/nano13091435.

(16) Sharma, H.; Sharma, S.; Sharma, C.; Paul, S.; Clark, J. H. Magnetically recoverable graphene oxide supported Co@Fe_3O_4/L-dopa for C-C cross-coupling and oxidation reactions in aqueous medium. *Mol. Catal.* **2019**, *469*, 27-39, https://doi.org/10.1016/j.mcat.2019.02.023.

(17) Mamontova, E.; Favier, I.; Pla, D.; Gómez, M. Chapter Two - Organometallic interactions between metal nanoparticles and carbon-based molecules: A surface reactivity rationale. In *Adv. Organomet. Chem.*, Pérez, P. J. Ed.; Vol. 77; Academic Press 2022; pp 43-103. https://doi.org/10.1016/bs.adomc.2022.01.004.

(18) Favier, I.; Toro, M.-L.; Lecante, P.; Pla, D.; Gómez, M. Palladium-mediated Radical Homocoupling Reactions: a Surface Catalytic Insight. *Catal. Sci. Technol.* **2018**, *8*, 4766-4773, https://doi.org/10.1039/C8CY00901E.

(19) Favier, I.; Pla, D.; Gómez, M. Palladium nanoparticles in polyols: synthesis, catalytic couplings and hydrogenations. *Chem. Rev.* **2020**, *120*, 1146-1183, https://doi.org/10.1021/acs.chemrev.9b00204.

(20) Garg, G.; Foltran, S.; Favier, I.; Pla, D.; Medina-González, Y.; Gómez, M. Palladium Nanoparticles Stabilized by Novel Choline-based Ionic Liquids in Glycerol Applied in Hydrogenation Reactions. *Catal. Today* **2020**, *346*, 69-75, https://doi.org/10.1016/j.cattod.2019.01.052.

(21) Leal-Duaso, A.; Favier, I.; Pla, D.; Pires, E.; Gómez, M. Design of Glycerol-Based Solvents for the Immobilization of Palladium Nanocatalysts: A Hydrogenation Study. *ACS Sustain. Chem. Eng.* **2021**, *9*, 6875-6885, https://doi.org/10.1021/acssuschemeng.1c01694.

(22) Liu, X.; Chen, L.; Xu, H.; Jiang, S.; Zhou, Y.; Wang, J. Straightforward synthesis of beta zeolite encapsulated Pt nanoparticles for the transformation of 5-hydroxymethyl furfural into 2,5-furandicarboxylic acid. *Chinese J. Catal.* **2021**, *42*, 994-1003, https://doi.org/10.1016/S1872-2067(20)63720-2.

(23) Tang, J.; Liu, P.; Liu, X.; Chen, L.; Wen, H.; Zhou, Y.; Wang, J. In situ encapsulation of Pt nanoparticles within pure silica TON zeolites for space-confined selective hydrogenation. *ACS Appl. Mater. Interfaces* **2020**, *12*, 11522-11532, https://doi.org/10.1021/acsami.9b20884.

(24) Duarte, T. A. G.; Favier, I.; Pradel, C.; Martins, L. M. D. R. S.; Carvalho, A. P.; Pla, D.; Gómez, M. Tetraalkylammonium functionalized hydrochars as efficient supports for palladium nanocatalysts. *ChemCatChem* **2020**, *12*, 2295 –2303, https://doi.org/10.1002/cctc.201902305.

(25) Wang, K.; Cui, W.; Bian, Z.; Liu, Y.; Jiang, S.; Zhou, Y.; Wang, J. Size and stability modulation of Pd nanoparticles on porous hypercrosslinked ionic polymer for heterogeneous

aerobic oxidative coupling of diaryl ether. *Appl. Catal. B* **2021**, *281*, 119425, https://doi.org/10.1016/j.apcatb.2020.119425.

(26) Gu, Y.; Bacchin, P.; Lahitte, J. F.; Remigy, J. C.; Favier, I.; Gómez, M.; Gin, D. L.; Noble, R. D. Catalytic membrane reactor for Suzuki-Miyaura C−C cross-coupling: Explanation for its high efficiency via modeling. *AIChE J.* **2017**, *63*, 698-704, https://doi.org/10.1002/aic.15379.

(27) López-Viveros, M.; Favier, I.; Gómez, M.; Lahitte, J.-F.; Remigy, J.-C. Remarkable catalytic activity of polymeric membranes containing gel-trapped palladium nanoparticles for hydrogenation reactions. *Catal. Today* **2020**, https://doi.org/10.1016/j.cattod.2020.04.027.

(28) Joshi, B. L.; Zielbauer, B. I.; Vilgis, T. A. Comparative study on mixing behavior of binary mixtures of cocoa butter/tristearin (CB/TS) and cocoa butter/coconut oil (CB/CO). *Foods* **2020**, *9*, 327, https://doi.org/10.3390/foods9030327.

(29) Wang, J.; Nie, R.; Xu, L.; Lyu, X.; Lu, X. Catalytic transfer hydrogenation of oleic acid to octadecanol over magnetic recoverable cobalt catalysts. *Green Chem.* **2019**, *21*, 314-320, https://doi.org/10.1039/c8gc03075h.

(30) Boetje, L.; Lan, X.; Silvianti, F.; van Dijken, J.; Polhuis, M.; Loos, K. More efficient synthesis and properties of saturated and unsaturated starch esters. *Carbohydr. Polym.* **2022**, *292*, 119649, https://doi.org/10.1016/j.carbpol.2022.119649.

(31) Pérez Alonso, A.; Mauriés, S.; Ledeuil, J.-B.; Madec, L.; Pham Minh, D.; Pla, D.; Gómez, M. Nickel Nanoparticles Immobilized on Pristine Halloysite: An Outstanding Catalyst for Hydrogenation Processes. *ChemCatChem* **2022**, *14*, e2022007, https://doi.org/10.1002/cctc.202200775.

(32) Reina, A.; Favier, I.; Pradel, C.; Gómez, M. Stable Zero-Valent Nickel Nanoparticles in Glycerol. *Adv. Synth. Catal.* **2018**, *360*, 3544-3552, https://doi.org/10.1002/adsc.201800786.

(33) Reina, A.; Pradel, C.; Martin, E.; Teuma, E.; Gómez, M. Palladium Nanoparticles Stabilised by Cinchona-based Alkaloids in Glycerol: Efficient Catalysts for Surface Assisted Processes. *RSC Adv.* **2016**, *6*, 93205-93216, https://doi.org/10.1039/C6RA19230K.

(34) Alcock, N. W.; Tracy, V. M.; Waddington, T. C. Acetates and acetato-complexes. Part 2. Spectroscopic studies. *J. Chem. Soc., Dalton Trans.* **1976**, 2243-2246, https://doi.org/10.1039/DT9760002243.

(35) Sui, R.; Lo, J. M. H.; Lavery, C. B.; Deering, C. E.; Wynnyk, K. G.; Chou, N.; Marriott, R. A. Sol–Gel-Derived 2D Nanostructures of Aluminum Hydroxide Acetate: Toward the Understanding of Nanostructure Formation. *J. Phys. Chem. C* **2018**, *122*, 5141-5150, https://doi.org/10.1021/acs.jpcc.7b12490.

(36) Nishikawa, M.; Kita, E.; Erata, T.; Tasaki, A. Enhanced magnetization in cobalt/magnesium oxide multilayer thin films. *J. Magn. Magn. Mater.* **1993**, *126*, 303, https://doi.org/10.1016/0304-8853(93)90609-6.

(37) Osuna, J.; de Caro, D.; Amiens, C.; Chaudret, B.; Snoeck, E.; Respaud, M.; Broto, J.-M.; Fert, A. Synthesis, Characterization, and Magnetic Properties of Cobalt Nanoparticles from an Organometallic Precursor. *J. Phys. Chem.* **1996**, *100*, 14571-14574, https://doi.org/10.1021/jp961086e.

(38) Meziane, L.; Salzemann, C.; Aubert, C.; Gérard, H.; Petit, C.; Petit, M. HCP cobalt nanocrystals with high magnetic anisotropy prepared by easy one-pot synthesis. *Nanoscale* **2016**, *8*, 18640-18645, https://doi.org/10.1039/C6NR05792F.

(39) Lozhkomoev, A. S.; Pervikov, A. V.; Kazantsev, S. O.; Suliz, K. V.; Veselovskiy, R. V.; Miller, A. A.; Lerner, M. I. Controlled Oxidation of Cobalt Nanoparticles to Obtain

Co/CoO/Co_3O_4 Composites with Different Co Content. *Nanomaterials* **2022**, *12*, 2523, https://doi.org/10.3390/nano12152523.

(40) Guo, B.; Xu, Y.; Zhou, S. Morphology dependence of low temperatures exchange bias Co/CoO core-shell nanoparticles/spheres by eco-friendly solvothermal route. *AIP Adv.* **2018**, *8*, 115115, https://doi.org/10.1063/1.5041017.

(41) Xie, X.; Ni, C.; Lin, Z.; Wu, D.; Sun, X.; Zhang, Y.; Wang, B.; Du, W. Phase and morphology evolution of high dielectric CoO/Co_3O_4 particles with Co_3O_4 nanoneedles on surface for excellent microwave absorption application. *Chem. Eng. J.* **2020**, *396*, 125205, https://doi.org/10.1016/j.cej.2020.125205.

(42) Srivastava, A. K.; Madhavi, S.; Menon, M.; Ramanujan, R. V. Synthesis of Co/Co_3O_4 Nanocomposite Particles Relevant to Magnetic Field Processing. *J. Nanosci. Nanotechnol.* **2010**, *10*, 6580-6585, https://doi.org/10.1166/jnn.2010.2532.

(43) Bucher, J. P.; Douglass, D. C.; Bloomfield, L. A. Magnetic properties of free cobalt clusters. *Phys. Rev. Lett.* **1991**, *66*, 3052, https://doi.org/10.1103/physrevlett.66.3052.

(44) van Schooneveld, M. M.; Kurian, R.; Juhin, A.; Zhou, K.; Schlappa, J.; Strocov, V. N.; Schmitt, T.; de Groot, F. M. F. Electronic Structure of CoO Nanocrystals and a Single Crystal Probed by Resonant X-ray Emission Spectroscopy. *J. Phys. Chem. C* **2012**, *116*, 15218-15230, https://doi.org/10.1021/jp302847h.

(45) Mei, D.; Zhang, B.; Liu, R.; Zhang, H.; Liu, J. Preparation of stearic acid/halloysite nanotube composite as form-stable PCM for thermal energy storage. *Int. J. Energy Res.* **2011**, *35*, 828-834, https://doi.org/10.1002/er.1874.

(46) Dijkstra, A. J. Kinetics and mechanism of the hydrogenation process - the state of the art. *Eur. J. Lipid Sci. Technol.* **2012**, *114*, 985-998, https://doi.org/10.1002/ejlt.201100405.

(47) Veldsink, J. W.; Bouma, M. J.; Schoon, N.-H.; Beenackers, A. A. C. M. Heterogeneous hydrogenation of vegetable oils: a literature review. *Catal. Rev. - Sci. Eng.* **1997**, *39*, 253-318, https://doi.org/10.1080/01614949709353778.

(48) De Oliveira Vigier, K.; Barrault, J.; Pouilloux, Y. Cis-trans isomerization of methyl cis-9-octadecenoate in the presence of cobalt tin catalysts. *J. Mol. Catal. A: Chem.* **2009**, *306*, 102-106, https://doi.org/10.1016/j.molcata.2009.02.033.

(49) Anneken, D. J.; Both, S.; Christoph, R.; Fieg, G.; Steinberner, U.; Westfechtel, A. Fatty Acids. 2006; Wiley-VCH Verlag GmbH & Co. KGaA. https://doi.org/10.1002/14356007.a10_245.pub2.

ACS Appl. Nano Mater. **2023**, DOI 10.1021/acsanm.3c01361
https://doi.org/10.1021/acsanm.3c01361

FOR TABLE OF CONTENTS USE ONLY

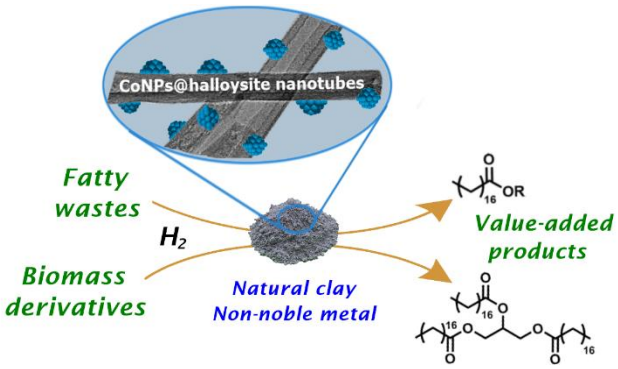

Cobalt nanoparticles immobilized on halloysite-based nanoclay led to efficient and highly selective C=C bond hydrogenation catalysts, including fatty waste valorization.